J Nanostruct 15(3): 1061-1074, Summer 2025

RESEARCH PAPER

The Role of Polymer Type on Linear and Nonlinear Behavior of Se Based Nanocomposites

Ahmad Abd Al Hussien [1], Kazem Jamshidi-Ghaleh [1], Kahtan A. Mohammed [2], Farzaneh Bayat [1]*

[1] *Department of Physics, Azarbaijan Shahid Madani University (ASMU), Tabriz, Iran*

[2] *Faculty of Pharmacy, Jabir Ibn Hayyan Medical University, Najaf, Iraq*

ARTICLE INFO

Article History:
Received 23 April 2025
Accepted 20 June 2025
Published 01 July 2025

Keywords:
Nanocomposite
Polymer
Synthesis

ABSTRACT

This study synthesised nanocomposites by incorporating selenium nanoparticles into polymeric materials, specifically polyethylene oxide (PEO), polyvinyl alcohol (PVA), and poly(methyl methacrylate) (PMMA). The investigation focused on their linear, nonlinear, structural, and formal optical properties. The properties of nanocomposites can be enhanced by incorporating them into polymeric materials appropriate for various applications. Nanocomposites are significant in nonlinear optics (NLO) owing to their substantial nonlinear response and broad spectral transparency. The three nanocomposites, Se+PEO, Se+PVA and Se+PMMA, were prepared and characterised through XRD, FESEM, EDX, FTIR, RSS, and PL techniques. The linear optical properties of the prepared samples were analysed using UV-VIS spectroscopy at various concentrations achieved through the addition of different polymers. The results indicated that an increase in concentration corresponded with a rise in absorbance at the same wavelength, with Se+PMMA exhibiting a higher absorbance compared to the other compounds. The fluorescence of all prepared samples was measured, and the results indicated that an increase in concentration led to a decrease in fluorescence. The Z-Scan technique, encompassing both open and closed aperture measurements, was employed to determine the nonlinear refractive index (n2) and the nonlinear absorption coefficient (β). The experiment utilised a solid-state diode laser operating at a wavelength of 405 nm and a power output of 2.94 mW. The Se+PMMA composite exhibits superior nonlinear behaviour compared to the other nanocomposites.

How to cite this article
Al Hussien A., Jamshidi-Ghaleh K., Mohammed K., Bayat F. The Role of Polymer Type on Linear and Nonlinear Behavior of Se Based Nanocomposites. J Nanostruct, 2025; 15(3):1061-1074. DOI: 10.22052/JNS.2025.03.023

INTRODUCTION

Nanomaterials science focusses on the design, synthesis, and characterisation of materials that possess at least one dimension within the nanoscale, typically ranging from 1 to 100 nanometres. Advancements in nanotechnology have led to the emergence of this field, allowing for the manipulation of matter at the nanoscale. Due to their unique physical, chemical, and mechanical properties compared to bulk materials, nanomaterials are widely utilised across multiple domains. Nanoparticles possess a high surface area to volume ratio, rendering them ideal for applications in energy storage, sensors, and catalysts. They are beneficial

* *Corresponding Author Email: Ahmedmaster915@gmail.com*

in biomedical, photonics, and electronics applications owing to their unique optical and electrical properties [1]. Nanomaterials exist in various forms, including quantum dots, nanowires, nanotubes, and nanoparticles. These resources can [2]. The examination of the toxicity and potential hazards associated with nanomaterials constitutes a significant area of study within nanomaterial science. In general, this sector is rapidly expanding, presenting numerous intriguing opportunities and challenges. Due to their diminutive size, shape-dependent electrical and plasmonic characteristics, and distinct optical properties, nanomaterials hold significant relevance in optics. Their capacity to engage with light in novel manners enables the development of innovative optical devices and applications for them [3]. The domain of plasmonics, which examines the interaction of light with surface plasmons in metallic nanostructures, has been shaped by nanomaterials. Plasmonics has enabled the development of novel sensors, imaging techniques, and optical communication systems. Metallic nanoparticle-based plasmonic sensors are proficient in detecting biological molecules and other analytes due to their ability to sense subtle changes in the refractive index or molecular binding events. Metamaterials, manmade structures capable of manipulating light in ways unattainable by natural materials, represent another application of nanoparticles in optics. Metamaterials possess negative refractive indices, enabling the development of optimal lenses and innovative devices for light manipulation [4]. Novel optical devices, such as nanoscale light-emitting diodes (LEDs), are being produced with nanomaterials for potential use in displays and lighting. They are also utilised to develop novel solar cells capable of capturing a broader spectrum of sunlight, rendering them more efficient than traditional silicon-based solar cells. Considering all factors, the unique optical properties of nanomaterials have led to significant breakthroughs in spectroscopy and optics, with potential applications in energy, communications, imaging, and sensing. [3] To optimise the utilisation of the nonlinear material, its nonlinearity must be accurately described. Numerous methodologies exist for assessing the nonlinearity of materials [3-7]. Nonetheless, a straightforward and accurate technique proposed by S. B. Mansoor et al. in 1989 is the z-scan approach [8,9]. The z-scan method depends on detecting the spatial displacement of an individual beam within the nonlinear medium to determine the nonlinear index of refraction (n2). Additionally, by quantifying the transmittance of an individual light beam traversing the nonlinear medium in relation to beam strength, the nonlinear absorption coefficient of the medium β can be ascertained. The beam intensity variation is obtained by scanning the nonlinear sample across the focal plane of the laser beam [8,9]. Nonlinear refraction is a consequence of the real component of the material's third-order susceptibility. This phenomenon results in the laser beam either focussing or defocusing depending on the sign of the refractive index (n2). Various physical mechanisms may account for this nonlinear characteristic, contingent upon the parameters of the nonlinear medium [10,11]. The characteristics of the medium dictate the importance of the generating mechanisms and the nonlinear refraction. Moreover, the nonlinear refraction is significantly affected by the environment of the nonlinear medium [12,13]. This phenomenon has been extensively examined across several materials [11-15]. The nature and intensity of solute nonlinearity are affected by solvent-solute interactions and the solvent's general physical properties. The temperature properties, polarity, and ability of the solvent to donate or receive a hydrogen bond may alter the nonlinearity of the solute [11-15].

MATERIALS AND METHODS

Materials

The PVA polymer (Merck, Germany), the PMMA polymer (United Kingdom), (ICI), the PEO polymer (Germany) and the Se element (INDIA) were used as received.

Methods

The two nanocomposites were synthesised as follows. Initially, we synthesised the polymers. PVA polymer was synthesised by incorporating 1 g of PVA into 100 ml of deionised distilled water using a homogeniser.

In a similar manner, 1 gramme of PMMA and PEO was dissolved in 100 mL of acetone and deionised distilled water, respectively. Subsequently, we synthesised the three nanocomposites, Se+PEO+PVA+PMMA, by including 0.01 g of each into 10 ml of PEO, PVA and PMMA, respectively. Subsequently, we allowed it to blend for approximately 50 minutes until thoroughly blended. The temperature inside the convection oven is 90 degrees Celsius. The first compound turned white -colored, whereas the second compound became lead and the third compound became black . This study used a continuous wave (CW) laser with a wavelength of 405 nm and Gaussian radiation as its light sources. A quartz cell with a thickness of 1 mm was employed to characterise the samples during the scanning experiment (Fig. 1).

RESULTS AND DISCUSSIONS

Field emission scanning electron microscopy (FESEM)

The polymer type influences molecular shape

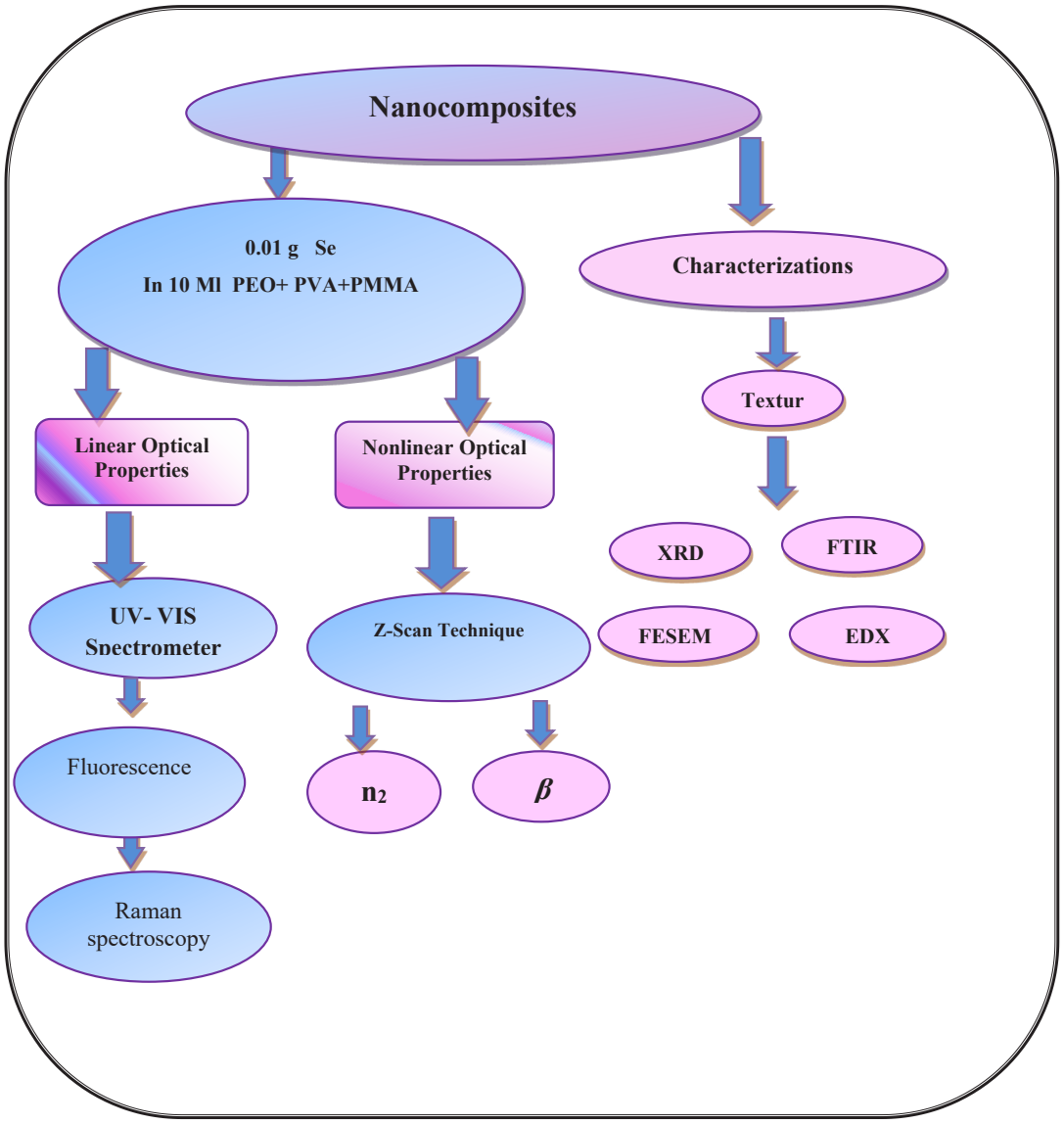

Fig. 1. The experimental procedure that is followed in this work.

and size, as longer polymer chains can coil more extensively, leading to smaller molecules. In chemical processes, polymers with robust interchain interactions typically yield bigger molecules compared to those with weaker interchain forces. In branching polymers, molecules exhibit more irregular geometries than linear polymers. The morphologies of Se + PEO, Se + PVA and Se + PMMA were examined using FESEM. In Fig. 2 the surface is almost spherical and rough which is due to the way the electrons interact with the uneven surface of the compound and mean diameters of particles are around 55 nm. Fig. 3 depicts a spherical surface form, with the particles exhibiting a rough and uneven texture. Consequently, we discovered that the molecules exhibit diverse shapes and sizes, and their surfaces are irregular. This results from the interaction of electrons with the compound's irregular surface, with mean particle sizes of 30 nm. Comparable outcomes are illustrated in Fig. 4. The surface morphology is spherical, and the particles exhibit a rough and uneven texture. Molecules exhibit many shapes and sizes, and their surfaces are irregular. This is once more attributable to the manner in which electrons engage with the irregular surface. The particle is spherical with a diameter of 30-50 nm. [12].

EDS Results

To investigate the Se. Chemical compositions, EDS measurements were performed on the

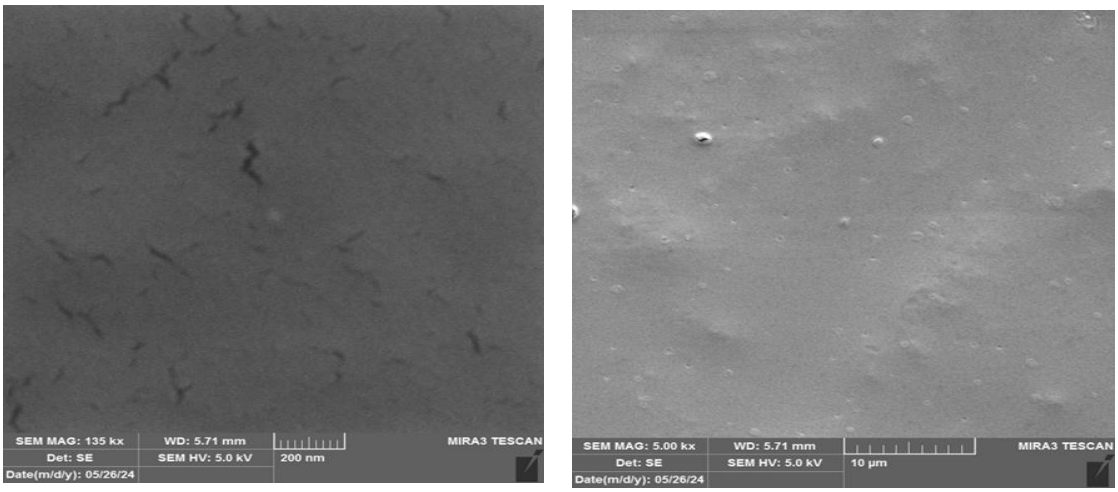

Fig. 2. FESEM image of Se +PEO.

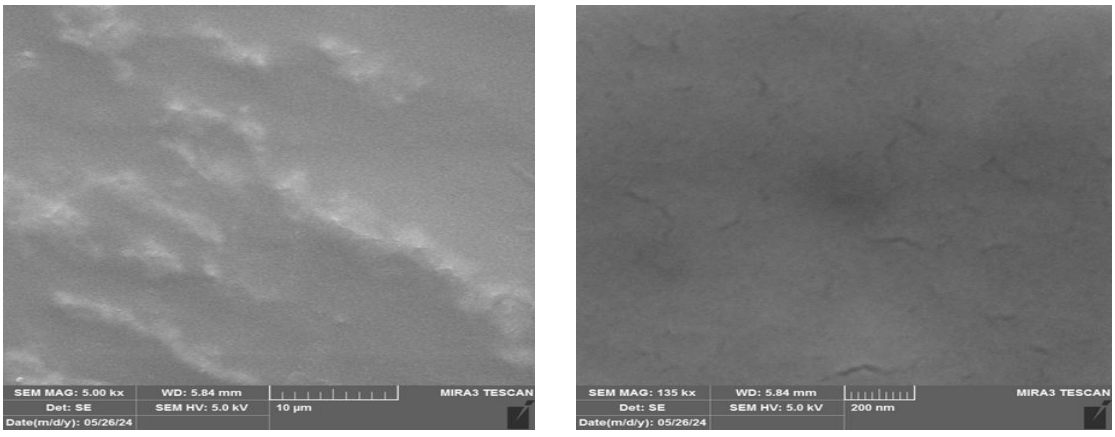

Fig. 3. FESEM image of Se +PVA.

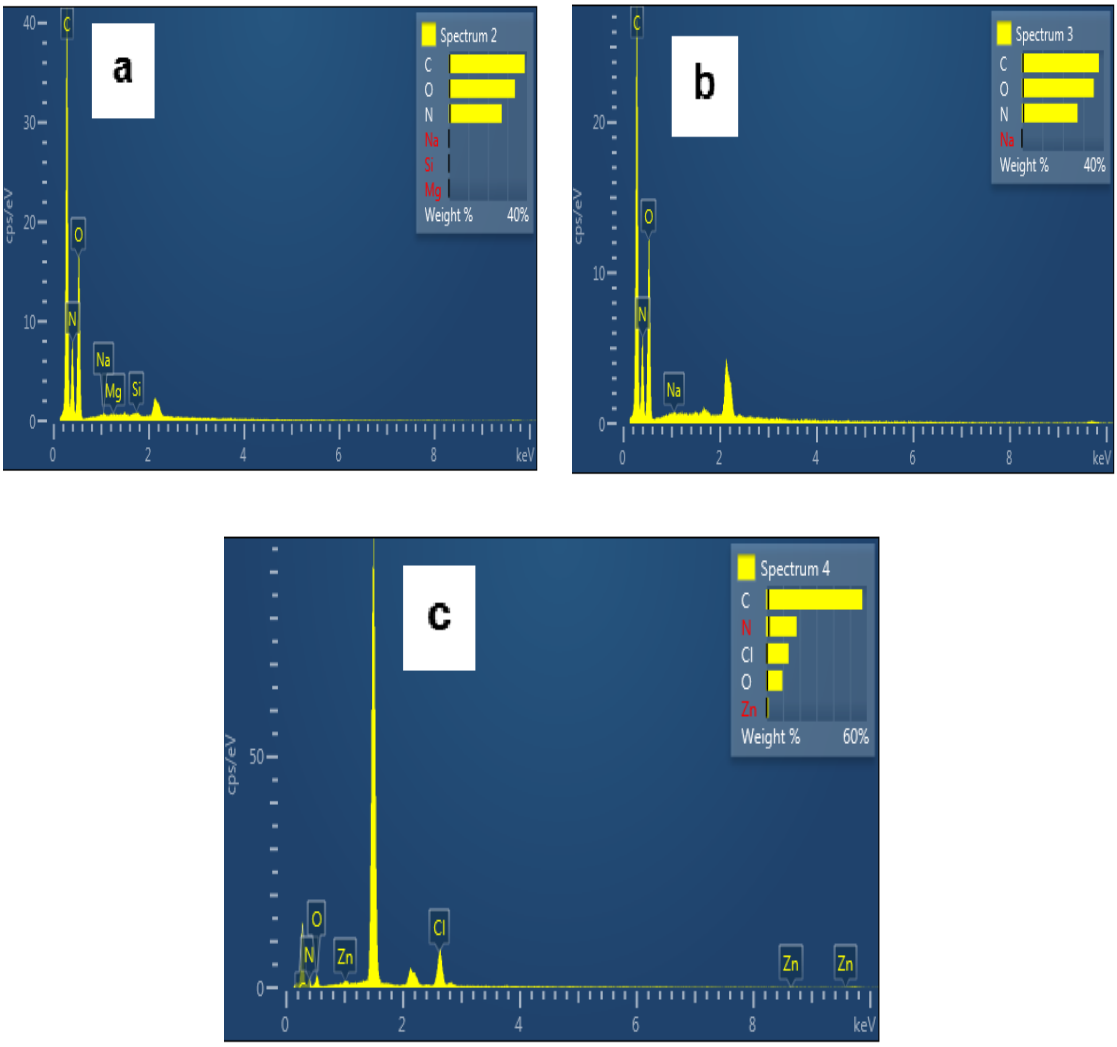

Fig. 5. Typical EDX spectra of(a) Se+PEO, (b) Se +PVA, and(c) Se +PMMA.

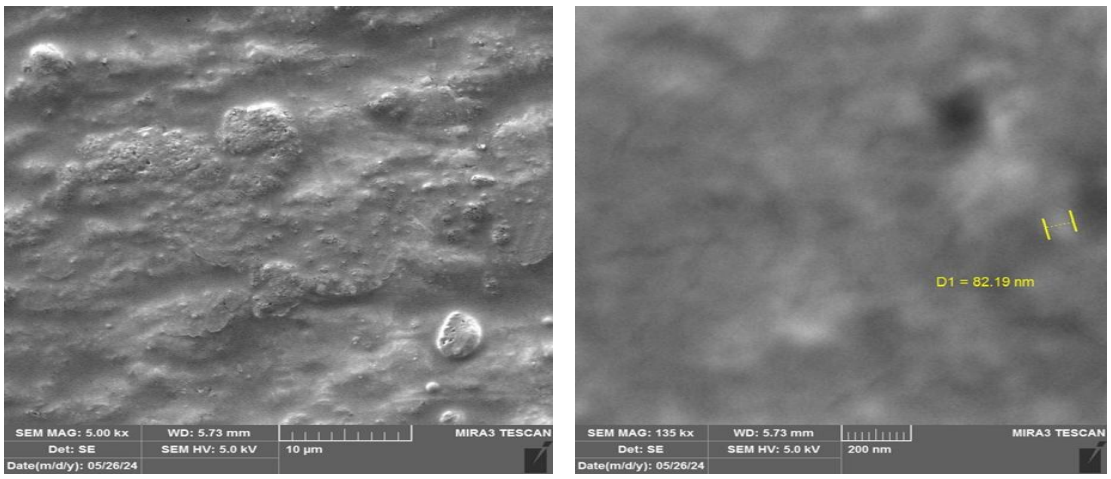

Fig. 4. FESEM image of Se+PPMMA.

samples. Fig. 5a shows the EDS spectra of Se +PEO. EDS patterns confirm the presence of sodium, magnesium and silicon in the compounds. Fig. 5b shows the EDS spectra of Se +PVA. EDS patterns approve the presence of sodium in the compounds. Fig. 5c shows the EDS spectra of Se+PMMA, and that the presence of zinc and chlorine in the compounds is confirmed. The single peak represents chlorine.

Raman Scattering Spectroscopy

The precise peak location frequency of each band was ascertained by Raman spectroscopy. To obtain the most precise Raman spectra, each spectrum was segmented into three peaks and analysed individually. Initially, the low-frequency domain is characterised by audio tones; thereafter, the medium-frequency domain features a blend of audio and optical phonons, as illustrated in Fig. 6a illustrates the quantity of high-frequency areas for the compound Se + PEO, characterised by sound phonons at (3000,3100,3200,3400, and 3500 cm^{-1}). The intensity of the peaks associated with the Raman modes connected to the vibrations of (N=C=O, N=N, C=N, O-H) varies. The rising quantity and peak intensity resulting from alterations in the compound's structure, which encompasses several molecular vibrations, leads to a high-frequency area , as illustrated in Fig. 6b illustrates the quantity of high-frequency areas for the compound Se + PVA, characterised by sound phonons at (2800, 3000, and 3400 cm^{-1}). The intensity of the peaks associated with the Raman modes connected to the vibrations of (N=C=O, N=N, C=N, O-H) varies. The rising quantity and peak intensity resulting from alterations in the compound's structure, which encompasses several molecular vibrations, leads to a high-frequency area. Fig. 6c illustrates the quantity of high-frequency regions for the compound Se + PMMA, which encompass sound phonons at (1800, 2000, 2400, 2800, 3000, and 3400 cm^{-1}).(b). As the number of peaks grows, the strength of the Raman modes associated with the vibrations of (N-N, C=H2, N=C=O, N=N, C=N, O-H) fluctuates. The compound's structural alteration leads to a high-frequency area due to numerous molecular vibrations. [13]

FTIR Spectra results

Fig. 7a illustrates the FTIR transmission spectrum of Se + PPEO. The extended regions with high peaks are approximately between 4000 and 400 cm^{-1}. The identified peaks correspond to the following functional groups and their corresponding ligands: Peak at 3368 cm^{-1}:O-H stretching in alcohols, phenols and carboxylic acids .Peak at 2944 cm^{-1}:CH stretching in alkanes . The peak at 2876 cm^{-1}: CH stretching in alkanes. The Peak at 1595 cm^{-1}:C=C stretching in alkenes and aromatic rings . The peak at 1486 cm^{-1}: C-H bending in alkanes.The Peak at 1322 cm^{-1}:O-H bending in carboxylic acids. The Peak at 1363 cm^{-1}: in-plane OH bending in alcohols and phenols. The Peak at 613 cm^{-1}:phosphate . The Peak at 470 cm^{-1}:M-O bending, where M is a metal cation [14].

Fig. 7b illustrates the FTIR transmission spectrum of Se + PVA. The elevated peak regions are situated between 3000 cm^{-1} and 2500 cm^{-1}. The peaks arise from C-H stretching vibrations. This bond transpires when a carbon atom shares two electrons with a hydrogen atom. The bond strength between carbon and hydrogen atoms

Table 1. Weight of element composition % of EDS resulting from Se added to PEO, PVA and PMMA.

Element	Se +PEO w%	Se +PVAw%	Se +PMMA w%
C	38.83	37.60	57.30
N	27.08	27.18	18.19
O	33.80	35.10	9.68
Na	15.40	0.12	-
Mg	0.03	-	-
Si	0.11	-	-
Cl	-	-	13.42
Zn	-	-	1.41

dictates the precise position of the peak on the wavenumber scale; absorption bands at 3300 cm^{-1} correspond to sp3 C-H stretches, whilst those near 3000 cm^{-1} belong to sp2 C-H stretches. The appearance of many peaks at 3000 cm^{-1} in the figure signifies that the molecule possesses various forms of C-H bonds. Aromatic and aliphatic C-H bonds typically exhibit peaks at around 3030 cm^{-1} and 2850 cm^{-1}, respectively [15].

Fig. 7c illustrates the FTIR transmission spectrum of Se +PMMA. The extended regions with high peaks range approximately 3000-3500 cm^{-1} and 1600-2000 cm^{-1}. These sections correspond to the functional groups in the molecule that vibrate when exposed to infrared radiation. We discover the large peak about 3000-3500 cm^{-1} due from vibrations. O-H expansion. This could be owing to the presence of alcohols, phenols, carboxylic acids or primary amines in the molecule. The broadening of the peak is owing to the possibility of variations in the hydrogen bonding environment. We detect the broad peak about 1600-2000 cm^{-1} due to the expansion of C=O (carbonyl). This may result from the presence of ketones, aldehydes, carboxylic acids, amides, or esters inside the molecule [14,15]. Reasons for

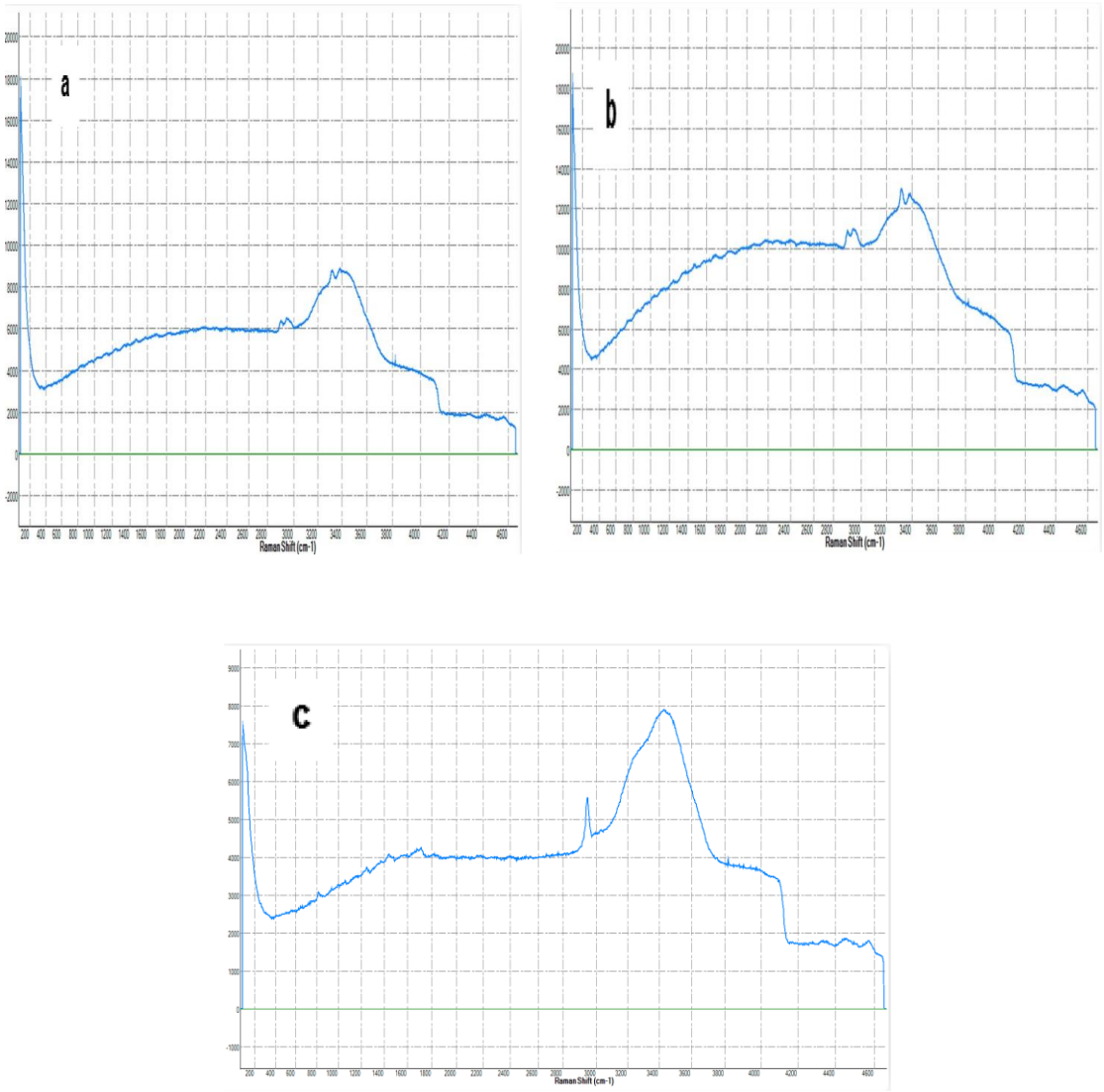

Fig. 6. Raman spectral for(a) Se+PEO, Se +PVA, and(c) Se+PMMA.

absorption in the FTIR spectrum:When the energy of a light wave corresponds to the vibrational energy of a molecular bond, the molecule is capable of absorbing light.This results in increased vibrational intensity of the connection. Various bonds oscillate at distinct frequencies. Consequently, various molecules absorb light at distinct wavelengths throughout the infrared spectrum [15,17, 18].

XRD results

The XRD technique is employed to determine the characteristics of the crystal structure and the predominant crystalline phases under specific conditions. This approach facilitates the identification of structural properties, including crystalline size and full width at half maximum (FWHM). The X-ray diffraction data for Se + PEO are illustrated in Fig. 8a. Numerous diffraction peaks are observed at 2θ values of 28.5°, indicating the presence of a crystalline component. The existence of various phases (amorphous and crystalline) can be validated by the appearance of broad peaks in conjunction with sharp peaks in the XRD analysis [18]. The X-ray diffraction data for Se + PVA are illustrated in Fig. 8b. Numerous diffraction peaks

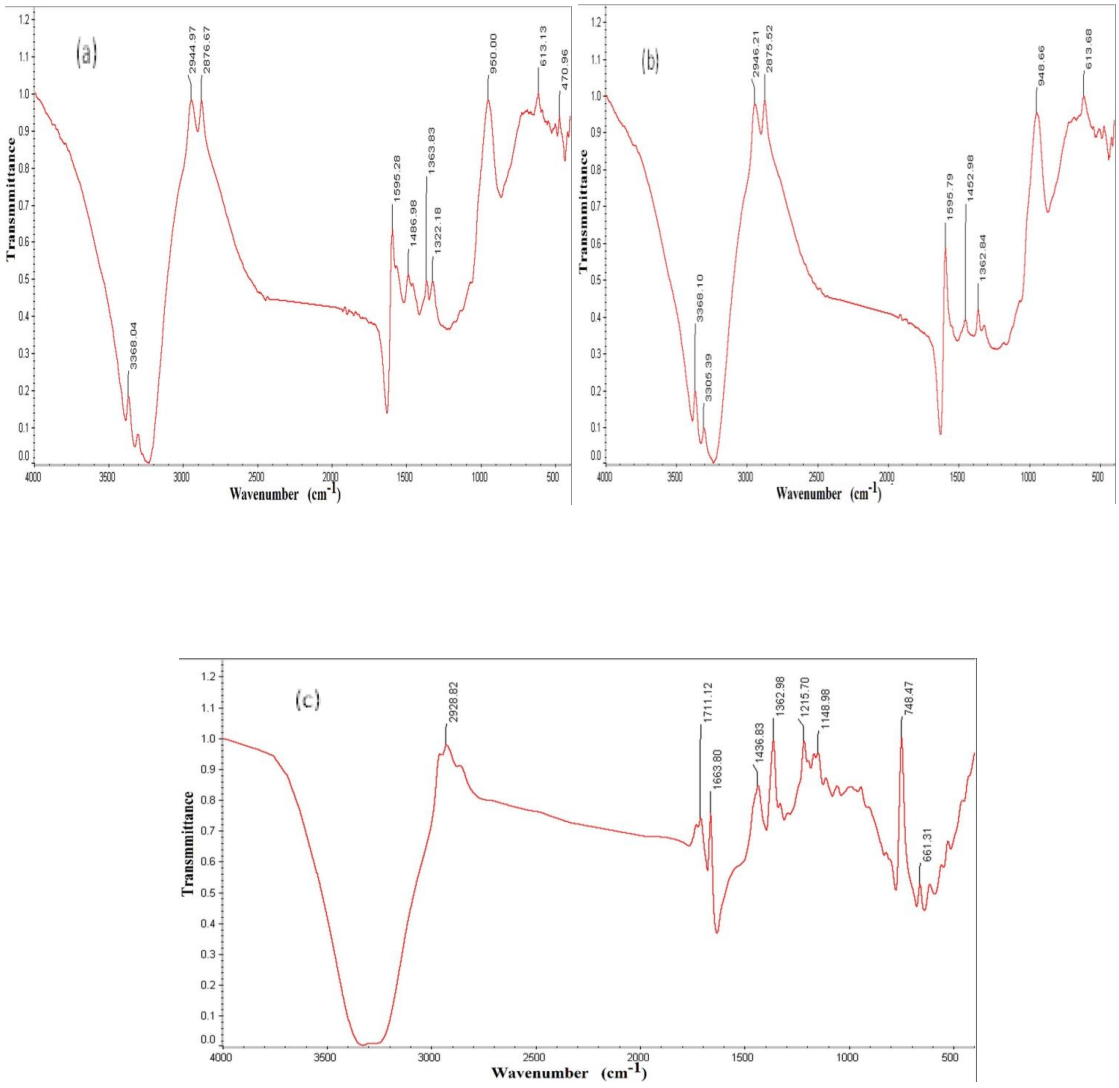

Fig. 7. FTIR spectrum of(a) Se +PEO, (b) Se +PVA, and(c) Se + PMMA.

are observed at 2θ values of 16°, 17.5°, 21.5°, 22°, 23°, 25.5°, 29.5°, and 36°, indicating the presence of a crystalline component. The existence of various phases (amorphous and crystalline) can be validated by the appearance of broad peaks in conjunction with sharp peaks in the XRD analysis. The substance produced exhibits exceptional purity, as the peak intensity serves as a definitive

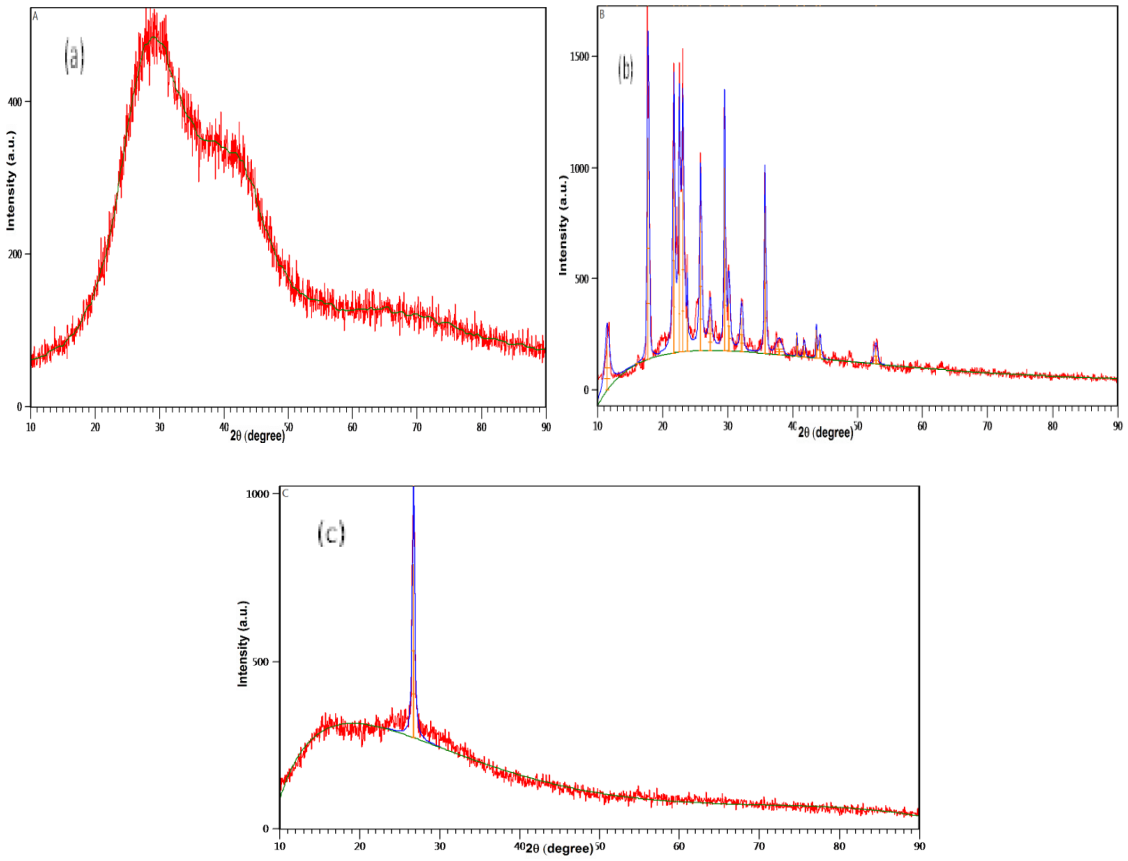

Fig. 8. XRD diffractions pattern for(a) Se+PEO, (b) Se +PVA, and(c) Se +PMMA.

Table 2. Interplaner space 'd', (h k l), middling micro strain in addition grainsize standards of Se + PEO, Se + PVA, and Se + PMMA.

Smple	2θ	D (nm)	FWHM (rad)	Gs (nm)	hkl
Se+PEO	28.5	3.1411	0.547	15	100
	16	5.2510	0.496	16	010
	22.240	3.9939	0.518	15	200
Se+PVA	23	3.8017	0.100	> 100	210
	25.5	3.5046	0.138	85	001
	29.5	3.0284	0.100	> 100	022
	36.073	2.4878	0.550	15	311
Se+PMMA	27.5	3.2356	0.375	22	111

indicator. The excellent crystalline quality of the synthesised nanoparticles may be verified [19]. Fig. 8c illustrates that X-ray diffraction for Se + PMMA can be investigated. The peak intensity occurs at 2θ=27.5°, and the presence of multiple phases (amorphous and crystalline) is suggested by the coexistence of broad and sharp peaks in the XRD. The high purity of the synthesised material is evidenced by the peak intensity, which serves as a definitive indicator of the favourable crystalline characteristics of the prepared nanoparticles [20]. The variation in angle values and (d) values, attributable to diverse compositions arising from the plurality of compound forms, signifies the presence of polycrystalline structures. The X-ray spectra data of the three chemicals indicate that they are crystalline, with some exhibiting nanoparticle characteristics. The presence of (NH-C=O) or the absorption band of (NH2) has resulted in enhanced regularity of atomic arrangement, facilitating the formation of crystalline size by aggregation, with crystalline dimensions observed in the nanometre range [21].

The following tables explain the reflection angles 2θ, the spacing between the reflective surfaces D, the average wave height FWHM, the crystalline size Gs and Miller indices hkl, the crystalline size Gs can be calculated according to (the Scherer equation) as follows [22]:

$$G_s = \frac{0.89\,\lambda}{FWHM\,\cos\theta} \quad (1)$$

Where FWHM is the full width at half maximum of XRD diffraction lines, θ is the reflection angle and λ is the wavelength of X-ray.

The sizes of particles, interplanar spacing distance and the average micro strain that estimate from different peaks were given in Table 2. From these results, the effect of capping agents is very clear and direct where the synthesized nanoparticles are highly pure.

Fluorescence Spectra Information

Following the preparation of three compounds and the acquisition of their absorption spectra, their emission spectra were documented utilising a fluorescence spectrometer. Fig. 9 illustrates the fluorescence spectra of selenium-doped PEO, PVA and PMMA polymers. At particular concentrations, the fluorescence intensity attains a specified value and thereafter diminishes with rising concentration. This conduct has been documented in the literature [23]. An increase in fluorescence intensity is observed upon the addition of polymers to selenium, indicating a rise in the concentration of the molecule. Consequently, fluorescence intensity increases; however, this enhancement is not sustained upon the addition of (Se+PMMA) due to the development of molecular aggregates. The agglomeration of complex molecules results in a reduction of the emission spectrum [23]. At reduced concentrations, indicated by the incorporation of Se + PVA, the electronic transitions (S1 to S0) are pronounced, resulting

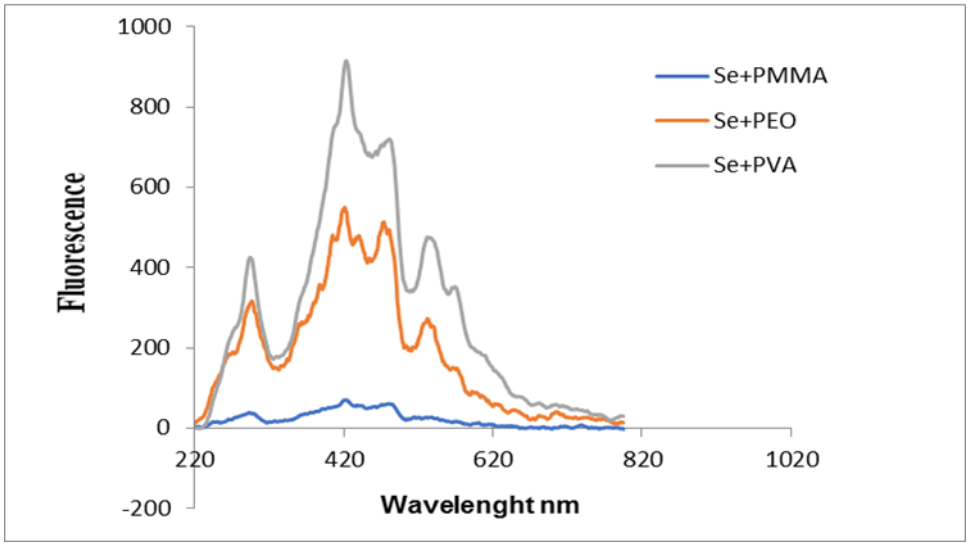

Fig .9. Photoluminescence spectra of Se+PEO, Se +PVA, and Se +PMMA.

in enhanced fluorescence. This approach is feasible; nevertheless, at elevated doses, it results in molecular aggregations of the chemical. The emission spectrum diminishes due to an increase in the rate of radioactive decay. Consequently, the image illustrates that as concentration rises, the peaks of the fluorescence spectra shift towards longer wavelengths, whereas the width of the fluorescence spectrum initially expands with increasing concentration before subsequently contracting.

Linear Optical Properties

Fig. 10 displays the linear absorption spectra of the nanocomposite samples generated. (a, b, c and d) The current results indicated that the absorption peaks changed to longer wavelengths following the addition of selenium (Se) to PMMA compared to the addition of polyvinyl alcohol (PVA). The electronic and vibrational states of the molecules near the contact induce this transition, enhancing the absorption of all molecules. This is anticipated to occur in nanocomposites within the ultraviolet (UV) spectrum due to the excitation of high-occupied molecular orbital (HOMO) electrons to low-occupied molecular orbital (LUMO). Nanocomposite samples demonstrate significant absorption in the ultraviolet region due to sufficient photon energy facilitating the transition of an electron from a lower to a higher energy state by the absorption of a photon of known energy. The fundamental absorption spectra illustrate band-to-band or excitation transitions. Each nanocomposite sample exhibits little absorption in the visible and near-infrared spectra. This phenomenon is elucidated by the inadequacy of input photon energy to engage with atoms; consequently, photons will propagate at a wavelength where the energy requisite for transmission decreases [24]. According to the findings in References [25], nanocomposites demonstrate superior linear optical properties compared to non-nanocomposites. Linear absorption coefficient (αo) and linear refractive

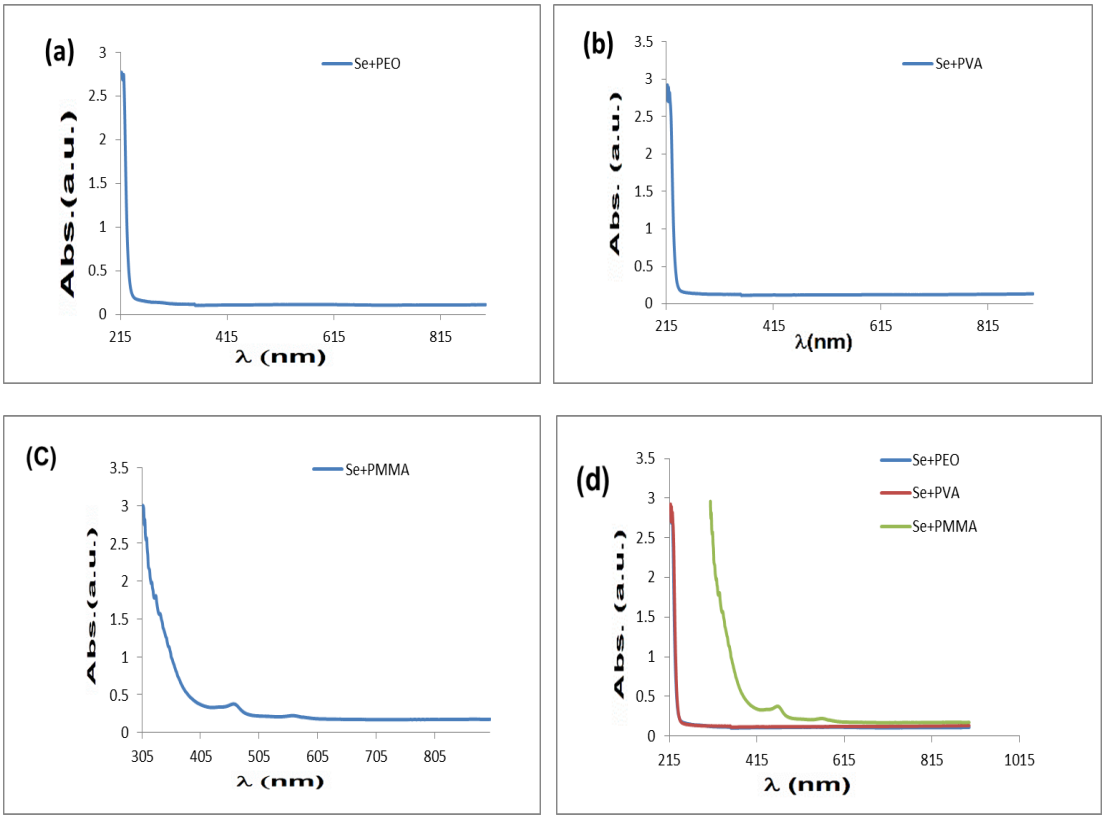

Fig. 10. Absorbance spectra for (a) Se + PEO, (b) Se + PVA, (c) Se + PMMA and (d) Se+PEO+PVA+PMMA.

index (NO). Table 1 indicates that the absorption values of Se + PMMA and Se+PVA exceed those of Se + PEO.

Non-Linear Optical Properties

The z-scan technique was employed to quantify the nonlinear refractive index and the nonlinear absorption coefficient through open and closed gap measurements. The normalised transmittance of Z-Scan measurements as a function of distance for selenium incorporated into to polyethylene glycol (Se+PEO), polyvinyl alcohol (Se+PVA) and polymethyl methacrylate (Se+PMMA) is depicted in Fig. 11a, b, c and d) The non-linear impact zone ranges from -4 mm to 4 mm. The apex succeeded by the trough of the transmittance curve derived from a closed aperture. Z-Scan data reveals a positive nonlinear refractive index (n2 > 0), resulting in lens autofocusing in these samples [26]. The low intensity of the transmitted beam and its relatively stable transmittance when the sample is out of focus elucidate the Z-Scan behaviour depicted in the preceding illustrations. The beam's intensity amplifies as the sample approaches its focal point, resulting in self-lensing of the sample, which aligns the beam above the far-field aperture and enhances the in situ transmittance measurement. The proportion of light incident on the detector will vary if the powerful laser beam induces a non-linear phase shift while traversing the focal zone. The strong laser beam induces self-lensing within the material. In this case, during sample translation, the detector's signal will display a peak and a trough. The nonlinear phase shift signal identifies the positions of the peak and valley relative to the z-axis, with the nonlinear phase shift conveyed by the beam being directly proportional to the variation in normal permeability from the curve's peak to its valley (ΔT_(P-V)). Moreover, as the beam defocuses or self-focuses, the resultant phase shift may be either positive or negative, contingent upon the nonlinear medium of transmission. The disparity in permeability between the apex and trough can be utilised to determine the extent of the phase shift. Self-defocusing results in a rise in the beam's aberration beyond the focal plane, leading to beam broadening upon focussing and a reduction in measured transmittance. The nonlinear refraction is minimal when out of focus (Z > 0), resulting in a transmittance that remains unaffected by Z. The produced samples demonstrate two-photon absorption in the open state and self-focusing behaviour in the closed state. These behaviours

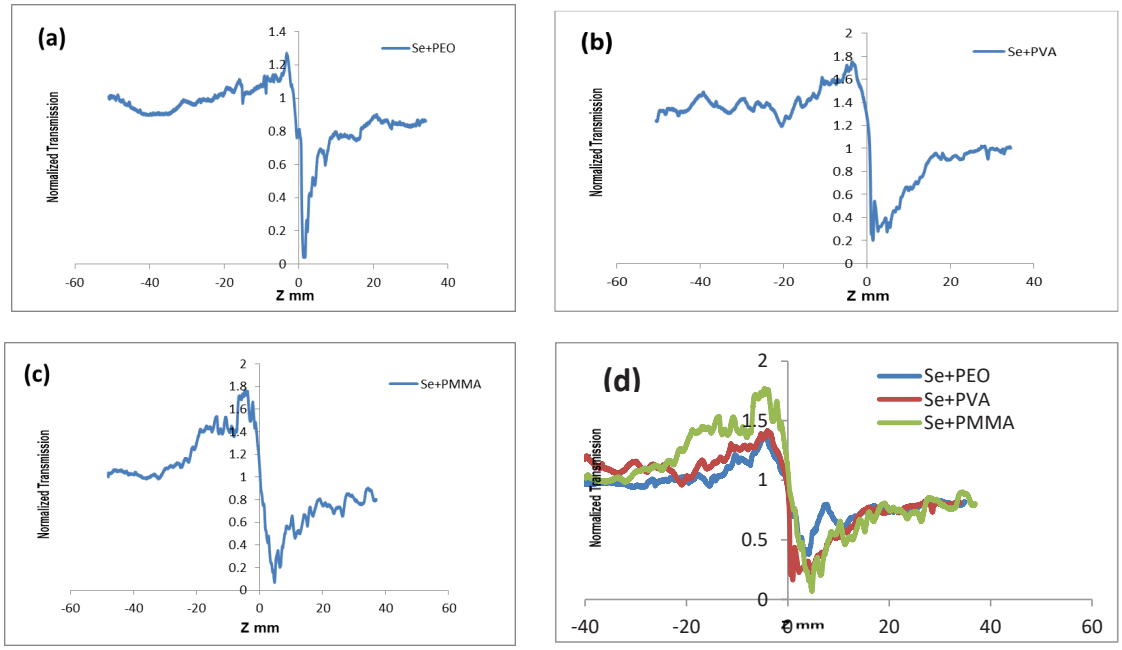

Fig. 11. Z-Scan data for (a) Se+PEO, (b) Se +PVA, (c) Se+PMMA and (d) Se+PEO+PVA+PMMA.

Table 3. The linear optical parameters. at λ=405 nm.

Materials	αo (cm^{-1})	Transmittance	Extinction Coefficient	Energy Gap(ev)	Absorption Coefficient
Se+PEO	0.918	0.1749	3.68E-06	6.0749	2.1164
Se+PVA	0.975	0.1187	3.87992E-06	6.4163	2.2457
Se+PMMA	0.987	0.1093	5.57422E-06	4.5757	2.2731

Table 4. Nonlinear optical parameters.

Materials	W.L. (nm)	Power (mW)	I_o (MW/m^2)	α (cm^{-1})	L_{eff} (m)	ΔT	n_2 (m^2/W)	n_o	$R_e\ \chi^{(3)}$ (e.s.u)
Se+PEO	405	12.7	85.660262	8.2942545	0.0009959	1.551532	2.98E-12	1.202362	1.0935E-06
Se+PVA	405	12.7	85.6603	9.01547733	0.00099551	2.8	2.31E-11	1.80098	1.9E-05
Se+PMMA	405	1.4	19.22297221	26.97557.35102	0.00099633	2.652632	2.27E-11	1.165362	7.81935E-06

align with prior findings [27, 28]. Tables 2 and 3 present the results of the nonlinear parameter calculations. The tables indicate that the values of the nonlinear parameter (n2) diminish with decreasing concentrations, (β) escalates as concentrations decline, and the linear parameters (Ia and αo) drop with lower concentrations. This results from the diminished quantity of molecules per unit volume at low concentrations. The closed-aperture Z-scan measures changeable transmittance values, which are utilised to ascertain the nonlinear phase transformation Δ Φo. The nonlinear behaviour of selenium included into PMMA polymer is greater than that of selenium incorporated into PVA polymer, and the latter is larger than the Se added to the PEO polymer ,corroborating the findings of References [27,28].

CONCLUSION

The nonlinear properties of selenium incorporated into (Se+PVA) and polymethyl methacrylate (Se+PMMA) were examined utilising the Z-Scan technique with a continuous wave solid-state diode laser operating at a wavelength of 405 nm and a power of 2.94 mW. Ultraviolet and visible spectroscopy were employed to ascertain the optical parameters, including transmittance, modulus, and refractive index for all samples. The nanoparticles were also analysed using X-ray diffraction (XRD), field emission scanning electron microscopy (FESEM), energy-dispersive X-ray spectroscopy (EDX), Fourier-transform infrared spectroscopy (FTIR), Raman spectroscopy (RSS), and photoluminescence (PL). FESEM examinations of nanocomposites revealed that their average size ranged from 30 to 55 nm, indicating their potential application in the production of highly sensitive nanomaterials, such as medical heat sensors. Absorption escalates with the rising concentration of the compound, as observed in polymers incorporated with selenium, where certain polymers exhibit enhanced absorption due to their elevated concentration. This aligns with the Beer-Lambert law, indicating that improved optical properties will be achieved with increased

concentration. The fluorescence diminishes linearly with rising chemical concentration, therefore rendering these samples suitable for optoelectronic applications. The nonlinear characteristics (β) and (n2) augment with rising concentrations of compounds, thereby enabling the utilisation of these compounds at such concentrations as an effective laser medium and for optical reduction applications. The linear refractive index (no) and linear absorption coefficient (αo) of all samples rise with increasing concentrations, thereby enabling their application as resonator cavities in liquid crystal lasers and other optical and photonic devices. The linear optical properties of Se +PMMA and Se+PVA surpass those of Se+PEO. The Se+ PMMA and Se +PVA nanocomposite exhibits superior nonlinear optical characteristics compared to the Se + PEO nanocomposite.

CONFLICT OF INTEREST

The authors declare that there is no conflict of interests regarding the publication of this manuscript.

REFERENCES

1. Huang T, Hao Z, Gong H, Liu Z, Xiao S, Li S, et al. Third-order nonlinear optical properties of a new copper coordination compound: A promising candidate for all-optical switching. Chemical Physics Letters. 2008;451(4-6):213-217.
2. Duerksen KM. Manual of Cutaneous Laser Techniques, 2nd ed. Archives of Ophthalmology. 2000;118(11):1595.
3. Maiman TH. Stimulated Optical Radiation in Ruby. Nature. 1960;187(4736):493-494.
4. Hall RN, Fenner GE, Kingsley JD, Soltys TJ, Carlson RO. Coherent Light Emission From GaAs Junctions. Physical Review Letters. 1962;9(9):366-368.
5. Lamb WE. Theory of an Optical Maser. Physical Review. 1964;134(6A):A1429-A1450.
6. Ippen EP, Shank CV, Dienes A. Passive mode locking of the cw dye laser. Applied Physics Letters. 1972;21(8):348-350.
7. Shank CV, Ippen EP. Subpicosecond kilowatt pulses from a mode-locked cw dye laser. Applied Physics Letters. 1974;24(8):373-375.
8. Hellwarth RW. Third-order optical susceptibilities of liquids and solids. Progress in Quantum Electronics. 1977;5:1-68.
9. Zel'dovich BY. "Principles of Lasers", by Orazio Svelto, translated from Italian by D. C. Hanna, Plenum Press, New York (1976). Soviet Journal of Quantum Electronics. 1978;8(4):550-551.
10. Laser Physics and Technology. Springer Proceedings in Physics: Springer India; 2015.
11. Symmetries in nonlinear optics. Nonlinear Optics: CRC Press; 2014. p. 115-136.
12. Sampreeth T, Al-Maghrabi MA, Bahuleyan BK, Ramesan MT. Synthesis, characterization, thermal properties, conductivity and sensor application study of polyaniline/cerium-doped titanium dioxide nanocomposites. Journal of Materials Science. 2017;53(1):591-603.
13. O Mousa A, H Nawfal S. Study of Electrical Properties of Photodetector. Journal Electrical Engineering and Science. 2017;3(2):11-18.
14. Frayne SH, Barnaby SN, Nakatsuka N, Banerjee IA. Growth and Properties of CdSe Nanoparticles on Ellagic Acid Biotemplates for Photodegradation Applications. Materials Express. 2012;2(4):335-343.
15. Thottoli AK, Unni AKA. Effect of trisodium citrate concentration on the particle growth of ZnS nanoparticles. Journal of Nanostructure in Chemistry. 2013;3(1).
16. Leal-Cruz AL, Vera-Marquina A, Espinoza-Duarte A, Rojas-Hernández AG, García-Juárez A, Aguilar-Martínez JA, et al. Optimization and synthesis approaches of semiconductor nanoparticles of crystalline CdSe using Taguchi method. Journal of Materials Science: Materials in Electronics. 2018;29(18):15801-15807.
17. LAS VEGAS SANDS CORP., a Nevada corporation, Plaintiff, Defendants. Gaming Law Review and Economics. 2016;20(10):859-868.
18. Farag AAM, Ashery A, Shenashen MA. Optical absorption and spectrophotometric studies on the optical constants and dielectric of poly (o-toluidine) (POT) films grown by spin coating deposition. Physica B: Condensed Matter. 2012;407(13):2404-2411.
19. Sohail M, Shah ZH, Saeed S, Bibi N, Shahbaz S, Ahmed S, et al. Hole transfer from CdSe nanoparticles to TQ1 polymer in hybrid solar cell device. Journal of Molecular Structure. 2018;1159:67-73.
20. Mathuri S, Ramamurthi K, Ramesh Babu R. Effect of Sb incorporation on the structural, optical, morphological and electrical properties of CdSe thin films deposited by electron beam evaporation technique. Thin Solid Films. 2018;660:23-30.
21. Sangamithirai D, Narayanan V, Stephen A. Synthesis and characterization of β-napthalene sulphonic acid doped poly(o-anisidine). AIP Conference Proceedings: AIP Publishing LLC; 2014. p. 1314-1315.
22. El Ghandoor H, Zidan HM, Khalil MMH, Ismail MIM. Synthesis and Some Physical Properties of Magnetite (Fe_3O_4) Nanoparticles. International Journal of Electrochemical Science. 2012;7(6):5734-5745.
23. Tafulo PAR, Queirós RB, González-Aguilar G. On the "concentration-driven" methylene blue dimerization. Spectrochimica Acta Part A: Molecular and Biomolecular Spectroscopy. 2009;73(2):295-300.
24. Jeyaram S. Nonlinear optical responses in organic dye by Z-scan method. Journal of Optics. 2022;51(3):666-671.
25. Geethu Mani RG, Ahamed MB. Laser performance of rhodamine B and methyl violet B base dye mixture in solid and liquid media. Journal of Nonlinear Optical Physics & Materials. 2014;23(04):1450053.
26. Henari FZ, Patil PS. Nonlinear Optical Properties and Optical Limiting Measurements of {(1Z)-[4-(Dimethylamino)Phenyl] Methylene} 4-Nitrobenzocarboxy Hydrazone Monohydrate under CW Laser Regime. Optics and Photonics Journal. 2014;04(07):182-188.
27. O Mousa A, H Nawfal S. Optical Properties of Porous Silicon Prepared at Different Etching Times. International Journal of Macro and Nano Physics. 2017;2(2):1-5.
28. Atta A, Abdeltwab E, Negm H, Al-Harbi N, Rabia M, Abdelhamied MM. Characterization and linear/non-linear optical properties of polypyrrole/NiO for optoelectronic devices. Inorganic Chemistry Communications. 2023;152:110726.